Research Article | Vol. 32, No. 27 / 30 Dec 2024 / Optics Express 48758
Optics EXPRESS

Controllable beam break-up, spectral broadening, and coherent beam recombination using arrays of singular beams

LYUBOMIR I. STOYANOV,[1,2,*] YINYU ZHANG,[2,3] ALEXANDER DREISCHUH,[1] AND GERHARD G. PAULUS[2,3]

[1]Department of Quantum Electronics, Faculty of Physics, Sofia University, 5, J. Bourchier Blvd., Sofia-1164, Bulgaria
[2]Institute of Optics and Quantum Electronics, Friedrich Schiller University, Max-Wien-Platz 1, D-07743 Jena, Germany
[3]Helmholtz Institute Jena, Fröbelstieg 3, D-07743 Jena, Germany
[*]l.stoyanov@phys.uni-sofia.bg

Abstract: The ever-increasing energy/power of modern laser sources is inevitably leading to new challenges and opportunities. One of them is the problem of spectral broadening of high-energy femtosecond pulses and their subsequent compression in time in, e.g., filaments. At high beam/pulse intensities, these tend to become unstable. One way to avoid such instabilities could be the controllable splitting of the beam into sub-beams. This, however, only makes sense if there is a reliable way to coherently recombine them. In this work, by using phase plates with etched arrays of optical vortices, we show an experimental realization of controllable femtosecond beam splitting, followed by nonlinear spectral broadening and a final coherent beam recombination. The results in ambient air and in a glass substrate confirm the feasibility of the proposed technique. Compression of the spectrally broadened pulses in glass down to the Fourier transform limit is demonstrated. All this provides a reasonable motivation for further optimization.

1. Introduction

Coherent beam combination (CBC) refers to a group of methods developed for achieving higher power/energy and for enhancing the spectral brightness of laser emission at preserved beam quality [1]. Generally, there are two sub-groups of methods for CBC – tiled-aperture and filled-aperture beam combination [2]. As indicated by the name, the mutual coherence including identical polarizations of the combined beams is a prerequisite. The probably simplest and most well-known example of the filled-aperture technique is the coherent combination of two beams from the two arms of an, e.g., Mach-Zehnder interferometer at its second beam splitter [3]. For proper alignment, destructive interference can be obtained in one of the interferometer outputs, while the interference in the other output will be constructive [3–5].

The tiled-aperture technique uses a phased array of coherent beams producing a total beam of a larger cross-section and of reduced divergence. In particular, fiber laser systems with high peak powers can use multiple amplification channels, which are subsequently coherently recombined [6]. This approach has been demonstrated with, e.g., 19- and 38-element fiber phased arrays [7], with 61 femtosecond fiber amplifiers [8], and with multicore fibers with a square array of 25 cores [9], just to mention a few. It is applicable for both laser diode arrays [10] and chirped-pulse amplification systems [11–13]. Generally, the methods for CBC are applicable from the continuous-wave to the femtosecond mode of laser operation [14,15] with applications ranging from processing quantum information [16] to coherent multidimensional spectroscopy [17] and to applications requiring high peak/average power [18]. Another related research

#539538 https://doi.org/10.1364/OE.539538
Journal © 2024 Received 15 Aug 2024; revised 30 Oct 2024; accepted 13 Nov 2024; published 23 Dec 2024

Optics EXPRESS

deserving attention is the divided-pulse nonlinear compression in a multipass cell recently demonstrated in [19]. In this work the authors presented an approach where the pulse-energy and peak-power limitations of a gas-filled multipass cell for nonlinear pulse compression are surpassed by applying a burst of four temporally separated pulses instead of one.

Here we propose a new approach for CBC based on the use of singular beams, more precisely arrays of optical vortices. Optical vortices (OVs, [20]) are the only truly two-dimensional singular beams [21,22]. An important characteristic of an optical vortex is its topological charge (TC). It is an integer number that indicates how many times, in units of 2π, the phase of the beam changes for one complete revolution around the axis of the beam. The sign of the TC depends on the direction of the phase change vs. the azimuthal coordinate. The TC of an OV can be erased, which leads to the recovery of the initial (Gaussian) beam profile in the Fourier plane [23].

The rich but often undesirable transverse dynamics of optical vortices placed on a common background beam (attraction and eventual annihilation of OVs with opposite TC, as well as repulsion and translation on the background when the TCs have the same signs) can be suppressed. To this end, OVs with periodically alternating signs of their TCs need to be arranged in large OV lattices. The result is a rigid transverse propagation of the OV lattices (arrays) [24].

The Fourier transformation of OV lattices in space, performed by a thin lens, is of particular interest for the present study. Specifically, a controllable splitting of such beams into an ordered structure of well-formed intensity peaks has been demonstrated in the focal plane of a lens (i.e. in the artificial far field) with square-shaped [25] and with hexagonal OV lattices [26] or even by mixing such singular OV lattices [27,28]. Similarly to isolated OVs, large OV arrays can be erased as well, and well-formed Gaussian beams are recovered in the artificial far field (see Figs. 5 and 6 in [25] and Figs. 4 and 5 in [26]). The above-mentioned beam reshaping techniques, along with their ability to controllably split the beam into sub-beams and later to recombine them, are the key component in the present approach to CBC. The intriguing question is what will happen when nonlinear processes leading to spectral broadening are introduced between the generation and annihilation of a vortex lattice.

In the context of this paper we are interested in the nonlinear evolution in continuous dielectric media that become weakly ionized by the propagating pulses. Beam filamentation is a complex nonlinear process (see e.g. [29,30]). This regime is reviewed in detail in [31] and should be distinguished from relativistic filamentation by very intense ($I>10^{17}$ W/cm^2) laser pulses in fully ionized media. In principle, the spectral broadening of the pulses in the course of e.g., femtosecond beam/pulse filamentation [32] is promising for subsequent pulse compression, provided there is a reliable way to coherently combine the sub-beams after filamentation. An essential argument in favor of the feasibility of this idea is the phase-locked white light continuum reported experimentally in [33].

In this work, by using phase plates with arrays of optical vortices, we show an experimental realization of controllable femtosecond beam splitting, followed by nonlinear spectral broadening of the sub-beams in ambient air and fused silica substrate, and a coherent recombination of the sub-beams. Even though, the approach slightly differs from the generally considered in the literature term for CBC, in the manner that in the intermediate step there is no amplification, rather than a self-action of the singular beams, it still demonstrates a powerful approach for beam recombination in space. Moreover, we have successfully compressed the initial 33-fs pulses to 20.5 fs (close to the estimated Fourier transform limit of 19 fs) for the case spectral broadening in a 3-mm fused silica plate (see Section 4).

2. Experimental setup and proof-of-principle measurement

This new concept for beam splitting and recombination is depicted in Fig. 1. An essential part of the physical background is the ability to manipulate (add, subtract, and, eventually, erase) the TC of an isolated OV [23] or even the TCs of large OV arrays composed of hundreds of OVs

Optics EXPRESS

[25–27]. Another important although well-known fact used, is that a thin lens performs a Fourier transformation of the incident laser beam with the artificial far field being in its focal plane.

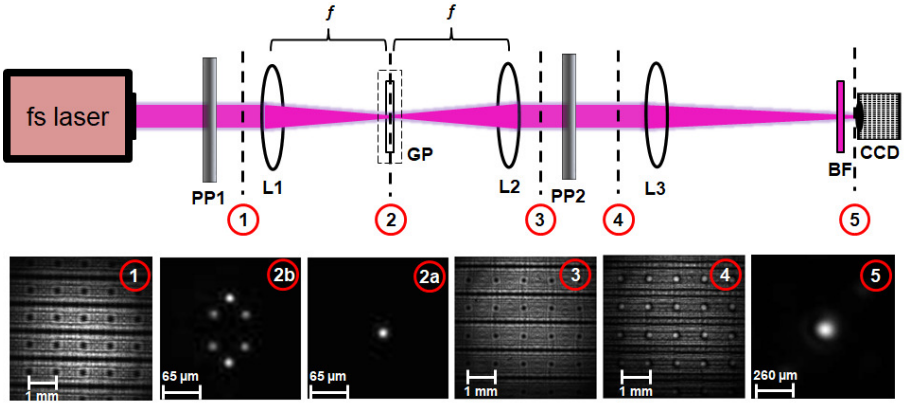

Fig. 1. Experimental setup: fs laser – Ti:Sapphire laser emitting 2.5-mJ, 38-fs pulses at a central wavelength of 780 nm. PP1, PP2 – phase plates of vortex arrays etched in fused silica; GP – 3 mm thick fused silica glass plate (used only for the experiments presented in Section 4); L1, L2 – converging lenses (f = 75 mm); L3 – converging lens (f = 500 mm); BF – interchangeable bandpass filters; CCD – charge-coupled device camera (1280 pix. × 1024 pix., pixel size 5.2 µm). **Numbered dashed lines** – planes of interest for which data from the proof-of-principle experiment in linear regime are shown below.

The optical scheme shown in Fig. 1 is expected to perform as follows: 2.5-mJ Ti:Sapphire laser pulses (diameter of the input beam – 4.2 mm (FWHM)) with a duration of 38 fs and a central wavelength of 780 nm are attenuated down to 1.2 mJ for creating the desired spectral broadening in air at atmospheric pressure (see Section 3) and below 250 µJ when using a 3 mm thick fused silica plate (Section 4). This was done in order to avoid instability in the spectrally broadened sub-beams in space until stable coherent beam recombination was reached in the desired wider spectral range. Custom-designed transmissive phase plates (PP1 and PP2) of vortex arrays etched in fused silica are placed on both sides of an 1:1 telescope formed by the lenses L1 and L2. The beam's numerical aperture is estimated to be of the order of 0.1-0.15 (depending on the case, air or glass plate). In view of the results presented in [34–36] this means that the external lens focusing has a bigger effect on propagation than the non-linear self-focusing. The used pulse energy, geometry and combination of lenses is chosen for keeping the spatial coherence of the OV lattices preserved, which is prerequisite for the coherent beam recombination afterwards. The specific structure of the phase plates (see also Fig. 2) producing the OV arrays results in 6 bright peaks in the Fourier plane. PP1 and PP2 are aligned such that all OVs created by PP1 are erased after PP2. Finally, lens L3 performs a spatial Fourier transformation of the beam which is captured by a CCD camera located precisely in the focal plane of L3. In front of the CCD camera a set of interchangeable bandpass filters are used for transmitting different spectral portions to study the quality of the recombined beam in these ranges.

In order to visualize the expected performance of the experimental setup we performed a proof-of-principle experiment in the linear regime. All planes of interest in Fig. 1 are indicated by numbered dashed lines in the experimental scheme. In frame 1, in the near field, one can see the obtained OV lattice at plane 1. In the artificial far field (plane 2), this square OV lattice transforms into 6 sub-beams (as shown in frame 2a). Frame 2b shows, just for comparison, the focused unmodulated Gaussian beam (when PP1 is removed from the setup). In the vicinity of plane 2, nonlinear spectral broadening of the focused sub-beams can be achieved in a millimeter-thin nonlinear medium (e.g. a glass plate) or in gas/air. Lens L2 performs the inverse Fourier

Optics EXPRESS

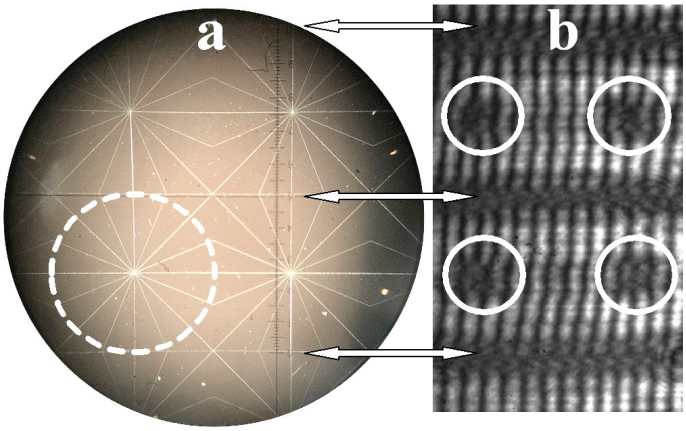

Fig. 2. (a) – Microscope photograph of a portion of the phase plate with the etched array of optical vortices with unit topological charges. Dashed circle – one OV of the array. Horizontal arrows – straight one-dimensional π-phase steps separating the rows of OVs. OV-to-OV distance – 1 mm. (b) – Interference pattern obtained with a continuous-wave laser beam transmitted through the vortex array and overlapped with a reference beam. White solid circles denote fork-like splittings of interference stripes indicative of the value and the signs of the TCs of the adjacent vortices.

transformation resulting in a recovered OV array (see frame 3, recorded in plane 3). If the geometry of PP2 is identical to the one of PP1, but the etched vortices are aligned to have opposite signs, all TCs of the OVs generated by PP1 will be erased. At the position of plane 4, the near-field intensity profile of the square-shaped OV lattice after both PPs (with already erased singularities, but with residual amplitude/intensity modulation) is shown. Lens L3 then performs the final Fourier transformation. When all TCs nested in the OV lattice after PP1 are erased by PP2, a well-formed Gaussian beam is recovered in its focus where the CCD-camera is located (Fig. 1, plane 5). This proof-of-principle measurement provides reasonable motivation to transfer the concept to experiments involving nonlinear processes (e.g., self-focusing, self-phase modulation, four-wave frequency mixing) induced by high-power femtosecond beams/pulses.

Figure 2(a) shows a microscope photograph of a portion of one of the phase plates with the etched array of optical vortices with unit topological charges. The dashed circle marks the position of one OV of the array etched in 16 discrete phase steps creating a 2π-phase ramp. Each row of OVs is separated from the neighboring one by a one-dimensional π-phase dislocation (see the white arrows in Fig. 2). The OV-to-OV separation is 1 mm. The diameter of each of the used phase plates is 3.8 cm. In panel (b) of Fig. 2 we show the interference pattern obtained with a continuous-wave laser beam (λ = 780 nm) transmitted through the phase plate and overlapped with a reference beam. The presence of the parallel 1-D dark beams created by the π-phase steps can be identified by the offset of the interference lines by a half of their period (see the arrows between panels (a) and (b)). The locations of the OVs in the interferogram (panel (b)) are marked with solid white circles. The fork-like splittings in opposing directions at the positions of adjacent phase dislocations clearly indicate unit topological charges of alternating signs. Such an arrangement of OVs phases in the phase plate guarantees that there will be no rotation of the generated OV array along its propagation direction.

3. Experimental data obtained in air

In panels (a-c) of Fig. 3 we show experimentally recorded energy density distributions (at the focal plane of L3) when only phase plate PP1 is aligned (a), when only PP2 is present (b), and in

Optics EXPRESS

the case of coherent beam recombination in ambient air when both PP1 and PP2 are aligned in the setup (c). The data was recorded with identical settings (exposure time etc.) on the CCD camera, i.e. the dynamic range of all images is the same. For better visibility, however, the upper halves of panels (a-b) are adjusted in brightness and contrast in the reproduction, while the respective dashed circles in the symmetric lower halves of these panels mark the positions of the remaining three focal peaks, where no such adjustments were made.

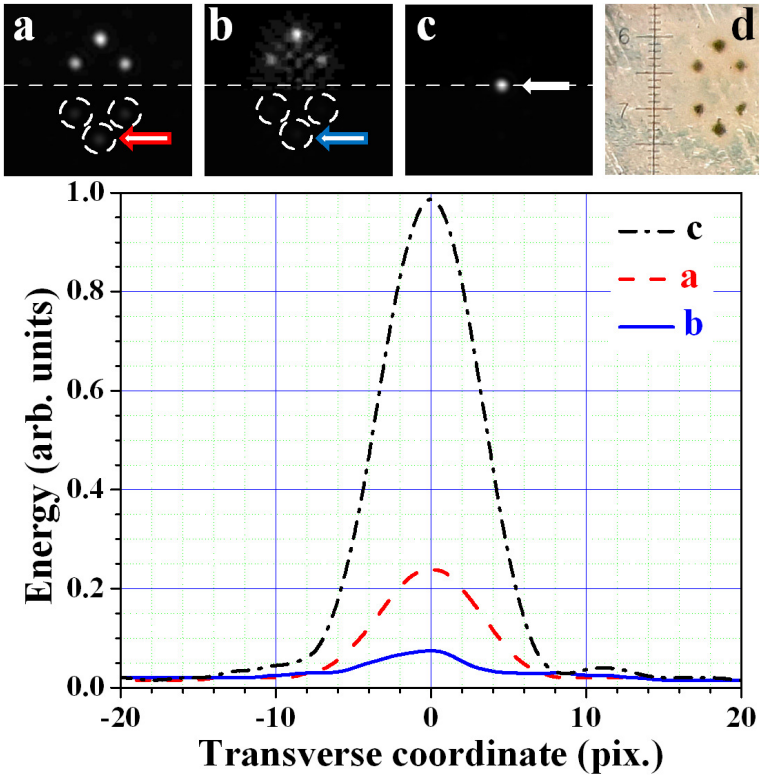

Fig. 3. Nonlinear medium – ambient air. Panels (a-c): Energy density distribution in the focal plane of L3, when phase plate PP1 is aligned only (a), when only PP2 is present (b), and in the case of coherent beam recombination when both PP1 and PP2 are aligned (c). The data are recorded in one and the same dynamic range. The upper halves of frames (a-c) (see white dashed line) are post-processed for better visibility. (d) – Microscope photo of the six-peak focal structure engraved in a clean aluminum foil in the focus of L1. Deduced vertical distance between the two left focal spots – 60 µm (scale division 10 µm). **Graph:** Horizontal cross-sections (along the marked arrows) of the raw data from the lowest peaks in panels (a) and (b) and of the central peak in panel (c) as originally recorded.

When only phase plate PP1 is present (panel (a)), six sub-beams are propagating in air and the spectrum is broadened in the beam waist of lens L1. Since PP2 is missing, the vortex array created by PP1 remains present in front of L3 and a well-formed six-peak structure is obtained in its focal plane and recorded by the camera. When only phase plate PP2 is present (see panel (b)), a single (Gaussian) beam is created in front of it, at more than five times higher intensity and the spectral broadening is accordingly larger. However, large spectral broadening appears to be incompatible with the fact that the PPs are designed for a single wavelength – here 795 nm. Accordingly, the spectral components deviating substantially from the design wavelength are expected to create fractional optical vortices (OVs with non-integer, i.e. with fractional TCs,

Optics EXPRESS

[37,38]) and grey 1-D dark beams instead of black dark beams. The Fourier transformation performed by the lens L3 for the OVs with fractional TCs does not result in well-shaped OVs and adds noise in the Fourier plane (the plane of the CCD camera). This is probably the origin of the structured low-level halo around the peaks in panel (b) of Fig. 3.

When both PPs are aligned in the system such that the OVs near the optimized wavelength of 795 nm are erased, then, interestingly, the fractional OVs and the 1-D phase dislocations of magnitude less than π are erased as well. As a consequence, the coherently recombined beam is well-shaped and of high contrast (Fig. 3(c)). The effect can be explained as follows: Due to the nonlinear evolution (self-phase modulation and four-wave mixing in the presence of self-focusing) the spectrum of the laser is broadened. This means that PP2 is illuminated with wavelengths that differ from the design wavelength of the plate. However, thanks to the four-wave frequency mixing a substantial part of the newly generated spectral components also carries the same phase dislocations as encoded by PP1 [39]. Because of this they can be erased by PP2 as well. A more detailed discussion of why this is possible is presented below in the context of Fig. 5.

The graph in Fig. 3 shows horizontal cross-sections through the lowest peaks of the energy density distribution shown in Fig. 3(a) and (b), as well as of the central peak shown in Fig. 3(c). As reported above, each of them is recorded within the same dynamic range of the camera and at the same output power of the laser. As can be seen, the peak of the coherently recombined beam (black dash-dotted curve) is about 4 times higher than the one recorded when only PP1 is present (red dashed curve) and around 13 times higher than the one when only PP2 is present (blue solid curve). The difference in the intensity between the blue solid curve and the red dashed curve is unexpected at first glance. However, one should not forget that in the case when only PP2 is present, a Gaussian beam is initiating the nonlinear process causing a strong broadening of the pulse spectrum. This means redistribution of the beam's intensity to the different spectral components. This is not the case when the laser is used at lower intensities, in linear regime of propagation. In this regime the blue solid curve and the red dashed curve are expected to overlap, which was confirmed experimentally, although not shown here.

It is interesting to know how many high-intensity sub-beams are formed in the presence of PP1. As mentioned, when PP1 is aligned, six focal peaks are created in the beam waist between lenses L1 and L2. By placing a piece of aluminum foil in the focus, we got the six burn traces shown in Fig. 3(d). The image in this panel clearly shows the fact that the upper and lower peaks of the six-peak structure are more intense than the remaining four ones. It is likely that not all six sub-beams create filaments, however we clearly identified filamentation by monitoring the transverse projection of the beam on a white screen.

Further, in the left part of Fig. 4 we show a comparison between the wavelength-integrated energy density beam distributions recorded by the CCD camera in the low intensity (linear; L) and in the moderate intensity (nonlinear; NL) regime. The notations of the columns mean that only phase plate PP1 is present (left column) or both PPs are aligned in the setup (right column). For better visibility all frames in Fig. 4 are processed individually in brightness and contrast. In the linear regime, we observed well-formed focal array of six bright peaks (Fig. 4, upper left frame) and as expected – the corresponding beam recombination is of excellent quality (upper right frame).

In the nonlinear regime, the presence of PP1 causes six high-intensity sub-beams to be formed. The red curve in the graph in Fig. 4 shows their spectrum. It is broader than the spectrum of the low intensity laser pulses shown by the black curve in the same graph. The broadening is not dramatic because the energy/intensity is redistributed over six peaks. However, the coherent recombination of the six spectrally broadened sub-beams created when both PPs are present (lower right panel in Fig. 4) is successful. The quality of the recombined beam in the non-linear regime is excellent and comparable to the quality observed in the linear case. For a reference, on the graph in Fig. 4 we also show the case when PP1 is absent. In this case, a single beam/pulse

Optics EXPRESS

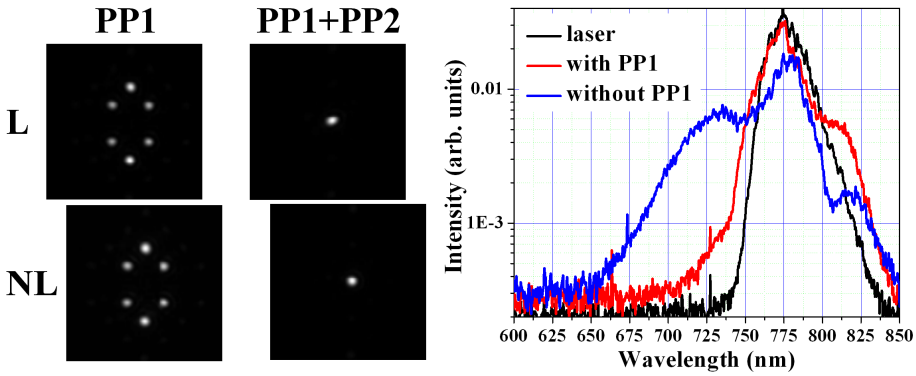

Fig. 4. Nonlinear medium – ambient air. Panels: Recorded energy density distributions in the plane of the CCD camera (focal plane of L3) when phase plate PP1 is present only (left panels), and when both PP1 and PP2 are aligned (right panels). Upper row – linear (L; low intensity) regime, lower row – nonlinear (NL) regime. **Graph:** Comparison between the input spectrum of the unfocused laser beam and the spectrum recorded at high intensity with vortex array PP1 (i.e. with six sub-beams). Just for a reference, the spectrum resulting from the nonlinear evolution of a single Gaussian beam when PP1 is absent is shown as well.

with higher intensity is propagating and the spectral broadening is accordingly larger (solid blue line).

An important note should be reminded and elaborated at this point: Generally, the self-phase modulation is considered as the main mechanism for spectral broadening in filaments. However, in this work the four-wave frequency mixing plays an important role ensuring that new spectral components carrying optical vortices are generated [39]. The 6 sub-beams will not coherently recombine after PP2, unless they carry phase profiles like those imprinted by PP1 on the input spectrum. One physical mechanism leading to the transfer of the phases of input OVs to the phases of newly generated spectral components is the (cascaded) four-wave mixing [39]. The experimental and theoretical results in this work confirm that topological charge conservation for (cascaded) nonlinear four-wave mixing process is fulfilled (also when self- and cross-phase modulation are present). The rule for the transformation of the topological charges follows the rule for the photon energy conversion. In the particular present case of OVs with unit TCs, the OVs in the newly-generated spectral components will carry unit TCs as well (see Figs. 3(a), 4(a), and 5(a) in [39]).

In order to characterize the coherently recombined beams in different spectral ranges, we used a set of interference bandpass filters placed right in front of the CCD camera (see Fig. 1). Below each column of frames in Fig. 5 the corresponding central wavelengths λ_c are indicated. The transmission bandwidths of all filters are ±20 nm. For better visibility, all frames are individually adjusted in brightness and contrast. We consider as interesting to show the reader how the obtained beam structures in the focus of lens L3 differ in the presence of only PP1, and when both PPs are used.

The upper row of frames in Fig. 5 presents the recorded energy density distribution in the focal plane of L3 recorded by a CCD camera when only PP1 is aligned in the setup. In the 650-nm-range, only two sub-peaks emit radiation (the most upper and lower peaks of the structure). They have relatively broad diffuse pedestals. In the 700-nm-range the remaining four peaks start emitting but their contribution to the overall spectral broadening seems to be relatively low. In the 750 – 770-nm range, where the spectral intensity of the incoming pulses is high, judging by the relative intensity of the peaks, the six sub-beams seem to emit. In the 790-nm-range the spectral intensity is even higher and ordered structure of weak satellite peaks, surrounding the

Optics EXPRESS

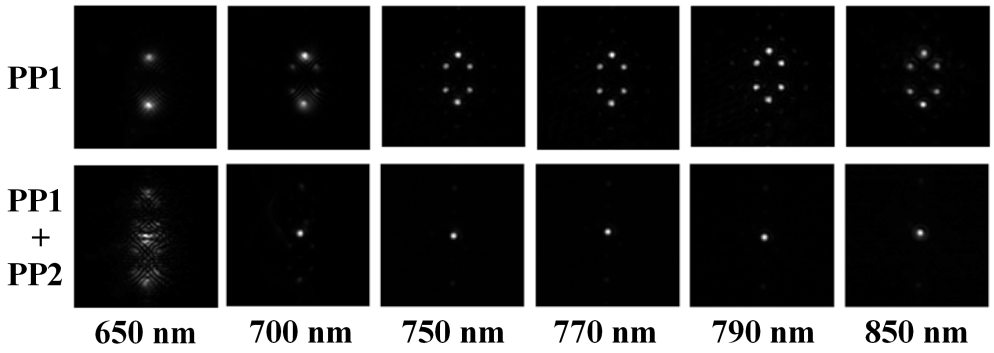

Fig. 5. Nonlinear medium – ambient air. Energy density distributions of the beams in the focal plane of L3 captured by a CCD camera in six spectral windows after the nonlinear evolution (see notations for the central wavelengths below each column of frames), when phase plate PP1 is present only (upper row of frames), and with both PPs aligned (lower row).

dominating six beams can be recognized. This is rather due to the high spectral intensity of the fundamental beam in this range. We do not think that these satellite peaks contribute noticeably to the spectral broadening. The well-formed six-beam structure is clearly expressed also in the 850-nm-range. Roughly speaking, when PP1 is aligned solely, the structure composed by six focal peaks in the plane of the CCD camera exists in a spectral range exceeding 100 nm.

When both vortex arrays are aligned in the setup, we experimentally recorded the frames shown in the lower row in Fig. 5. In the 650-nm-range the observed structure is noisy and, despite the middle bright structure, the beam recombination is not successful. This can be attributed to the combined effect of losing spatial coherence between the sub-beams and the large offset of this spectral range from the wavelength for which the PPs are designed. In the 700-nm-range a peak corresponding to a coherently recombined beam is clearly dominating the weak satellites. Above 700 nm and up to 850 nm the quality of this peak improves. As a partial conclusion, in view of the above results one can state that the coherent recombination of the beams in the plane of the CCD camera after their nonlinear spectral broadening in air is successful in a spectral range exceeding 150 nm. These results encouraged us to continue the study with solid state nonlinear medium.

4. Experiment in a glass substrate

The experimental setup we used for obtaining the results in this section is the same as this in Fig. 1. The only difference (Fig. 1, dashed rectangle) is the fused silica plate used as nonlinear medium located in the beam waist between lenses L1 and L2 and the 4.8 times reduced pulse energy (around 250 μJ). The alignment of the former 1:1 telescope (L1-L2) is kept unchanged and the CCD camera is slightly shifted to the new focal plane of lens L3. The use of solid-state substrates can appear preferable because of their higher third-order nonlinearities and lower thresholds for self-focusing (see e.g. [40]).

Microscope photo of the surface of the fused silica substrate shown in the left part in Fig. 6 proves that in the presence of PP1, in the nonlinear regime and when the substrate retains its position, all six sub-beams are able to damage the substrate's surface. Moreover, it can easily be recognized that the damages caused by the most upper and lower focal peaks are larger compared to those caused by the other four peaks, thus proving again their higher intensities. It is also evident that, when PP1 is removed, the Gaussian beam with significantly higher intensity causes considerably larger damage. For each of the further presented measurements we used a fresh surface of the glass plate and reduced the mean beam power below the damage threshold.

Optics EXPRESS

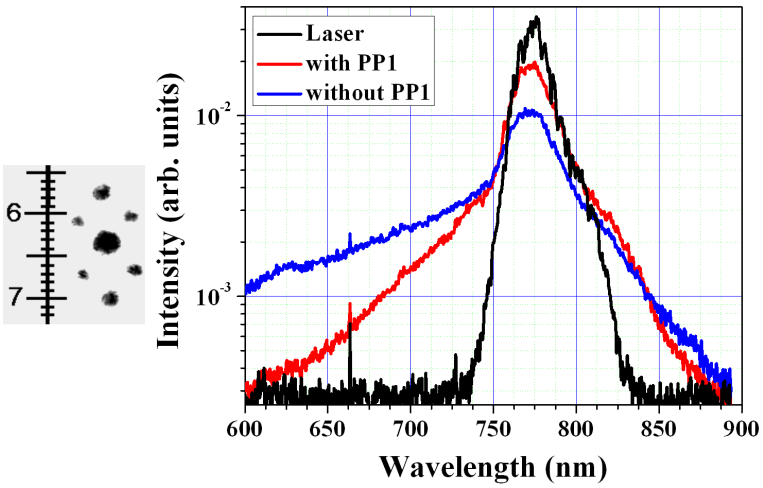

Fig. 6. Nonlinear medium – fused silica. Left. Microscope photograph of intentional damages burnt in the fused silica substrate. The central damage is caused by the unmodulated laser beam (when PP1 removed). When PP1 is present, six outer-lying burns, resulting from the formation of six intense sub-beams are seen. Deduced vertical distance between the two left focal spots – 60 µm, (scale division 10 µm). **Graph.** Comparison between the input spectrum of the unfocused laser and the spectrum recorded at high intensity with vortex array PP1 (i.e. with six sub-beams). Just for a reference, the spectrum resulting from the focused Gaussian beam (when PP1 is absent) is shown as well.

Further, we present a comparison between the input spectrum of the laser and the spectra recorded at high intensity. On the graph in Fig. 6 the spectrum of the laser beam/pulses at low intensity (black curve) is compared with the spectrum broadened when 6 sub-beams are formed at high intensity (red curve; PP1 present) and (just for a demonstration) with the even broader spectrum, when a single intense Gaussian beam is present (blue curve; PP1 removed). The much larger spectral broadening when PP1 is removed is an expected effect. When PP1 is present, the short-wavelength spectral broadening in the glass plate is well-pronounced as compared to the input spectrum of the laser (black curve) and it is much larger as compared to the spectral broadening in ambient air (see also the graph in Fig. 4).

It is interesting to show how this relatively big spectral broadening initiated by the six sub-beams in the glass substrate is influencing the beam recombination in the focal plane of L3. A comparison between the wavelength-integrated energy density beam distributions recorded by the CCD camera in the low intensity (linear; L) and in the nonlinear (NL) regime is shown in Fig. 7. The notations of the columns mean that only PP1 is present (left column), or both PPs are aligned in the setup (right column). In the NL regime, the obtained results with one PP show six dominating peaks surrounded by a diffuse halo of self-focused peaks diffracting until reaching the CCD camera. However, the coherent beam recombination after the controllable beam break-up and nonlinear evolution in this high intensity regime is of a reasonably good quality and is comparable to this in linear regime (second column of frames in Fig. 7). The obtained results support the idea to controllably split the beam using arrays of singular beams, then initiate spectral broadening and finally to coherently recombine the already spectrally broadened beam.

As a next step in the experiment, we recorded and analyzed the coherently recombined beams in the focus of lens L3 by filtering different spectral ranges and recording the respective energy density distributions of the beams. The respective data are shown in Fig. 8. The transmission bandwidths of the filters are the same as in the experiment in air.

Optics EXPRESS

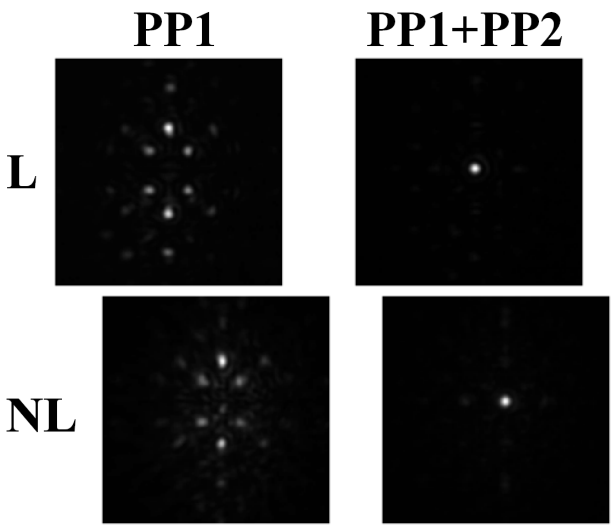

Fig. 7. Nonlinear medium – fused silica. Recorded energy density distributions in the plane of the CCD camera (essentially the focal plane of L3) when phase plate PP1 is present only (left panels), and when both PP1 and PP2 are aligned (right panels). Upper row – linear (L; low intensity) regime, lower row – nonlinear (NL) regime. Each panel is individually post-processed in brightness and contrast for better visibility.

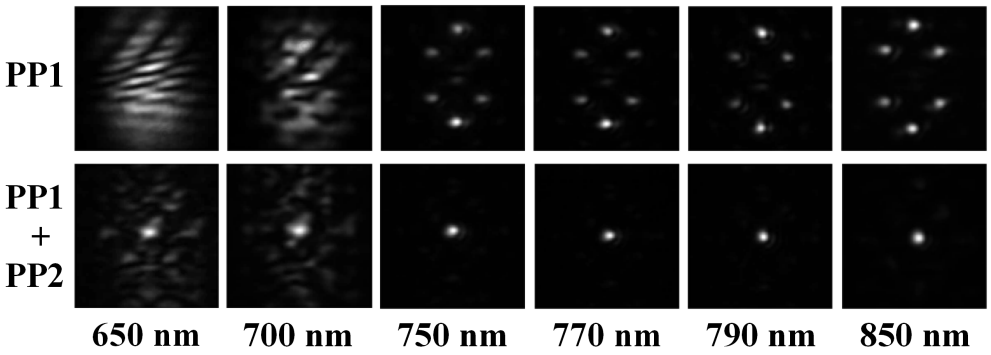

Fig. 8. Nonlinear medium – fused silica. Energy density distributions of the beams in the focal plane of L3 (captured by a CCD camera) in six spectral ranges of the broadened spectrum due to the nonlinear evolution (see the notations for the central wavelengths below each column of frames) when phase plate PP1 is present only (upper row of frames), and with both PPs aligned (lower row).

In the case when only phase plate PP1 is present (Fig. 8, upper row of frames), in the 650 – 700-nm-range one can see a clear signature of the beam's self-focusing, fission and partial loss of spatial coherence. When both PPs are present (lower left frames), the situation is different. A clear central peak resulting of the recombination of the coherent part of the beam is dominating the surrounding low-intensive halo. In this halo, particularly in 650-nm-range (see Fig. 8, leftmost lower frame), some of the peaks mimic the six-peak structure originating when PP2 is illuminated by newly generated spatial components for which the spatial coherence in the course of the nonlinear process is lost.

Optics EXPRESS

When only PP1 is aligned, in the 750 – 850-nm range, where the spectral intensity of the incoming pulses is high, six sub-beams are well formed, with the most upper and most lower peaks dominating (Fig. 8). This is evident from the relative intensity of the peaks. In these experiments with fused silica substrate as a nonlinear medium, when PP1 is aligned solely, the structure composed by six focal peaks in the plane of the CCD camera exists in a 100-nm-interval as obtained with ambient air.

The essential positive result in the experiment with fused silica is presented in the second row of frames shown in this figure, where we show data recorded when both vortex arrays are aligned in the setup. In the 750 – 850-nm-range, a well-formed peak corresponding to a coherently recombined beam is clearly dominating the weak satellites. In view of the above, one can state that the coherent recombination of the beams in the plane of the CCD camera after their spectral broadening in fused silica is successful in a range exceeding 100 nm, similar to the obtained in air (however, in a broader 150-nm interval).

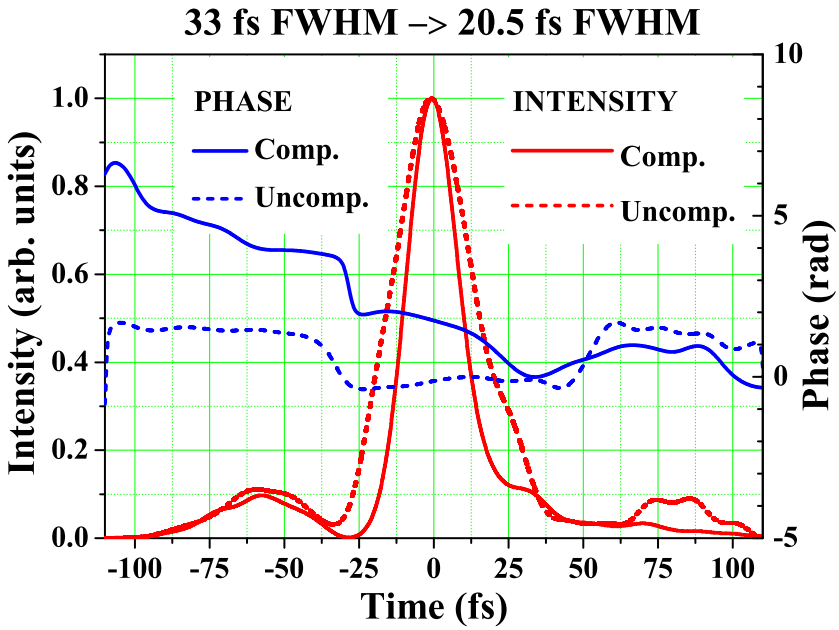

Fig. 9. Pulse compression following the coherent beam recombination. Intensity (red curves) and phase (blue curves) of the uncompressed laser pulses (dashed curves) and of the compressed pulses after nonlinear spectral broadening in glass and external pulse-compression in a setup with chirped-mirrors (solid curves). Pulse duration before compression – 33 fs (FWHM). Duration of the compressed pulse – 20.5 fs (FWHM).

One important point which has not been addressed so far is what happens with the coherently recombined beams/pulses in the temporal domain. In order to answer this question, we performed a pulse compression experiment by sending the spectrally broadened pulses to a double-angle chirped-mirror setup. A pair of fused silica wedges was inserted to fine tune the dispersion. The pulse duration of the recombined pulse was characterized with a commercial SPIDER device performing spectral phase interferometry for direct electric-field reconstruction. For obtaining pulses close to the Fourier-transform limit (FTL), the dispersion needs to be elaborately controlled. To this end, the position of the compressor in the chirped-pulse-amplification section of the laser system was optimized to deliver 33 fs pulses. In this way, we successfully compressed these 33-fs input pulses (subsequently spectrally broadened in a 3-mm fused silica plate), down to 20.5 fs

Optics EXPRESS

(close to the estimated FTL of 19 fs). The last is clearly demonstrated in Fig. 9, where the input and the compressed pulses and their phases are compared. Further pulse compression requires much more efforts on controlling different factors in the compression system, e.g., the pulse energy, the thickness and the position of the plate, additional chirped mirrors, fine group delay dispersion tunability of the input pulse and etc., which will be investigated in the future.

5. Conclusion

In the presented work, we used a phase plate with an etched vortex array to intentionally split a femtosecond laser beam into six sub-beams in the focus of a lens. This beam reshaping technique is controllable and is based on singular optics. Its reversibility is exploited in order to coherently recombine the sub-beams. Specifically, a recollimating lens and a second phase plate aligned in such a way to erase all phase dislocations created by the first phase plate were used. Then a focusing lens performs the final beam focusing and recombination. After the nonlinear evolution (spectral broadening) of the pulses in ambient air and in a fused silica substrate, we experimentally observed successful sub-beams coherent recombination in ranges exceeding 150 nm in air and 100 nm in glass. One possible physical mechanism of transferring the phase dislocations encoded by the first phase plate into the newly generated components is the coherent four-wave frequency mixing. The possibility to successfully compress the input laser pulses, spectrally broadened in glass, down to the FTL is also demonstrated. The estimated efficiency on the exit of the system (ratio between the power measured behind the last focusing lens L3 and the power in front of the first phase plate PP1) is 76% for the experiments in ambient air and around 63% in the case when fuse-silica plate was used. The efficiency can be improved, since the losses are trivial in the sense that they are mainly caused by Fresnel reflections from the uncoated surfaces of some of the optical elements. The proposed technique will allow to achieve better pulse-to-pulse stability when pulses with higher intensities are used if the beam/pulse is split into larger number of ordered focal peaks. One way to do this is to use a different vortex array, in the manner that the topological charge of every single optical vortex in the array is higher. Such vortex arrays are successfully generated and reported (see e.g. Fig. 22 in [41]). In our view, the results confirm the feasibility of the proposed technique and provide a reasonable motivation for further optimization and investigation.

Funding. Bulgarian National Science Fund (КП-06-Н78/6); Deutsche Forschungsgemeinschaft (PA 730/16-1); Ministry of Education and Science (project ELI ERIC BG, National Roadmap for Research Infrastructures).

Acknowledgements. The authors gratefully acknowledge the contribution of P. Hansinger at the stage of designing the used phase plates. The work of L. S. and A. D. was also supported by the European Union-NextGenerationEU, through the "National Recovery and Resilience Plan of the Republic of Bulgaria, project BG-RRP-2.004-0008-C01". L. S. would like to gratefully acknowledge the research scholarship granted by the Alexander von Humboldt Foundation. This research was also supported from LASERLAB-EUROPE (grant agreement no. 654148, EU's Horizon 2020 research and innovation programme).

Disclosures. The authors declare no conflicts of interest.

Data availability. The datasets generated and analyzed during the current study are available from the corresponding author upon a reasonable request.

References

1. Z. Liu, P. Zhou, X. Xu, *et al.*, "Coherent beam combining of high power fiber lasers: Progress and prospect," Sci. China Technol. Sci. **56**(7), 1597–1606 (2013).
2. V. E. Leshchenko, "Coherent combining efficiency in tiled and filled aperture approaches," Opt. Express **23**(12), 15944–15970 (2015).
3. R. Paschotta, "Coherent beam combining," https://www.rp-photonics.com/coherent_beam_combining.html (2020).
4. M. Tempus, W. Lüthy, and H. P. Weber, "Coherent recombination of laser beams with interferometrical phase control," Appl. Phys. B: Lasers Opt. **56**(2), 79–83 (1993).
5. M. Fabert, M. Săpântan, K. Krupa, *et al.*, "Coherent combining of self-cleaned multimode beams," Sci. Rep. **10**(1), 20481 (2020).

Optics EXPRESS

6. A. Klenke, E. Seise, J. Limpert, *et al.*, "Basic considerations on coherent combining of ultrashort laser pulses," Opt. Express **19**(25), 25379–25387 (2011).
7. J. Zuo, F. Zou, X. Zhou, *et al.*, "Coherent combining of a large-scale fiber laser array over 2.1 km in turbulence based on a beam conformal projection system," Opt. Lett. **47**(2), 365–368 (2022).
8. I. Fsaifes, L. Daniault, S. Bellanger, *et al.*, "Coherent beam combining of 61 femtosecond fiber amplifiers," Opt. Express **28**(14), 20152–20161 (2020).
9. N. A. Kalinin, E. A. Anashkina, G. Leuchs, *et al.*, "Lenslet array-free efficient coherent combining of broadband pulses at the output of a multicore fiber with a square core grid," Opt. Express **30**(2), 1013–1020 (2022).
10. S. M. Redmond, K. J. Creedon, J. E. Kansky, *et al.*, "Active coherent beam combining of diode lasers," Opt. Lett. **36**(6), 999–1001 (2011).
11. A. Heilmann, J. L. Dortz, L. Daniault, *et al.*, "Coherent beam combining of seven fiber chirped-pulse amplifiers using an interferometric phase measurement," Opt. Express **26**(24), 31542–31553 (2018).
12. A. V. Andrianov, A. V. Kim, E. A. Anashkina, *et al.*, "Modeling of coherent beam combining from multimillijoule chirped pulse tapered fiber amplifiers," Eur. Phys. J. Spec. Top. **224**(13), 2579–2583 (2015).
13. C. Peng, X. Liang, R. Liu, *et al.*, "Two-beam coherent combining based on Ti:sapphire chirped-pulse amplification at the repetition of 1 Hz," Opt. Lett. **44**(17), 4379–4382 (2019).
14. S. J. McNaught, P. A. Thielen, L. N. Adams, *et al.*, "Scalable coherent combining of kilowatt fiber amplifiers into a 2.4-kW beam," IEEE J. Sel. Top. Quantum Electron. **20**(5), 174–181 (2014).
15. T. Zhou, T. Sano, and R. Wilcox, "Coherent combination of ultrashort pulse beams using two diffractive optics," Opt. Lett. **42**(21), 4422–4425 (2017).
16. G. D. Jimenez, V. G. Garces, and K. A. O'Donnell, "Coherent reconstruction of pump beams through recombination of entangled photon pairs," Phys. Rev. A **99**(2), 023853 (2019).
17. D. B. Turner, K. W. Stone, K. Gundogdu, *et al.*, "Invited article: The coherent optical laser beam recombination technique (COLBERT) spectrometer: Coherent multidimensional spectroscopy made easier," Rev. Sci. Instrum. **82**(8), 081301 (2011).
18. T. Fan, "Laser beam combining for high-power, high-radiance sources," IEEE J. Sel. Top. Quantum Electron. **11**(3), 567–577 (2005).
19. H. Stark, C. Grebing, J. Buldt, *et al.*, "Divided-pulse nonlinear compression in a multipass cell," J. Phys. Photonics **4**(3), 035001 (2022).
20. G. A. Swartzlander and C. T. Law, "Optical vortex solitons observed in Kerr nonlinear media," Phys. Rev. Lett. **69**(17), 2503–2506 (1992).
21. M. Soskin and M. Vasnetsov, "Chapter 4 - Singular optics," in *Progress in Optics*, vol. 42 of *Progress in Optics* E. Wolf, ed. (Elsevier, 2001), pp. 219–276.
22. G. R. Allan, S. R. Skinner, D. R. Andersen, *et al.*, "Observation of fundamental dark spatial solitons in semiconductors using picosecond pulses," Opt. Lett. **16**(3), 156–158 (1991).
23. L. Stoyanov, S. Topuzoski, I. Stefanov, *et al.*, "Far field diffraction of an optical vortex beam by a fork-shaped grating," Opt. Commun. **350**, 301–308 (2015).
24. A. Dreischuh, S. Chervenkov, D. Neshev, *et al.*, "Generation of lattice structures of optical vortices," J. Opt. Soc. Am. B **19**(3), 550–556 (2002).
25. L. Stoyanov, G. Maleshkov, M. Zhekova, *et al.*, "Far-field pattern formation by manipulating the topological charges of square-shaped optical vortex lattices," J. Opt. Soc. Am. B **35**(2), 402–409 (2018).
26. L. Stoyanov, G. Maleshkov, M. Zhekova, *et al.*, "Far-field beam reshaping by manipulating the topological charges of hexagonal optical vortex lattices," J. Opt. **20**(9), 095601 (2018).
27. L. Stoyanov, G. Maleshkov, M. Zhekova, *et al.*, "Controllable beam reshaping by mixing square-shaped and hexagonal optical vortex lattices," Sci. Rep. **9**(1), 2128 (2019).
28. L. Stoyanov, G. Maleshkov, I. Stefanov, *et al.*, "Focal beam structuring by triple mixing of optical vortex lattices," Opt. Quantum Electron. **54**(1), 34 (2022).
29. A. Braun, G. Korn, X. Liu, *et al.*, "Self-channeling of high-peak-power femtosecond laser pulses in air," Opt. Lett. **20**(1), 73–75 (1995).
30. M. Scheller, M. S. Mills, M.-A. Miri, *et al.*, "Externally refuelled optical filaments," Nat. Photonics **8**(4), 297–301 (2014).
31. A. Couairon and A. Mysyrowicz, "Femtosecond filamentation in transparent media," Phys. Rep. **441**(2-4), 47–189 (2007).
32. R. Dorsinville, P. Ho, J. Manassah, *et al.*, "Applications of Supercontinuum: Present and Future," in *The Supercontinuum Laser Source*, (Springer-Verlag, 2006), pp. 377–398.
33. M. Bellini and T. W. Hänsch, "Phase-locked white-light continuum pulses: toward a universal optical frequency-comb synthesizer," Opt. Lett. **25**(14), 1049–1051 (2000).
34. K. Lim, M. Durand, M. Baudelet, *et al.*, "Transition from linear- to nonlinear-focusing regime in filamentation," Sci. Rep. **4**(1), 7217 (2014).
35. D. Reyes, M. Baudelet, M. Richardson, *et al.*, "Transition from linear- to nonlinear-focusing regime of laser filament plasma dynamics," J. Appl. Phys. **124**(5), 053103 (2018).
36. D. V. Pushkarev, G. E. Rizaev, and L. V. Seleznev, "Nonlinear to geometric focusing transition: beam self-cleaning and self-focusing critical power," J. Opt. Soc. Am. B **41**(8), 1732–1738 (2024).

Optics EXPRESS

37. G. Maleshkov, D. N. Neshev, and A. Dreischuh, "Nonlinear beam steering by fractional vortex dipoles," Phys. Rev. A **80**(5), 053828 (2009).
38. G. Maleshkov, P. Hansinger, N. Dimitrov, *et al.*, "Branching optical signals by fractional vortex dipoles," Opt. Commun. **285**(16), 3529–3534 (2012). Special Issue: Sub-wavelength Light Localization and Focusing.
39. P. Hansinger, G. Maleshkov, I. L. Garanovich, *et al.*, "Vortex algebra by multiply cascaded four-wave mixing of femtosecond optical beams," Opt. Express **22**(9), 11079–11089 (2014).
40. A. Brodeur and S. L. Chin, "Ultrafast white-light continuum generation and self-focusing in transparent condensed media," J. Opt. Soc. Am. B **16**(4), 637–650 (1999).
41. L. Stoyanov, S. Topuzoski, G. G. Paulus, *et al.*, "Optical vortices in brief: introduction for experimentalists," J. Phys. Photonics **138**(8), 702 (2023).